one finds Compositae, chenopods (goosefoot), Gramineae (grasses), Caryophyllaceae, *Ephedra* (types *dystachya* and *fragilis*), Dipsacaceae, *Artemisia*, and several others.

The arboreal pollens are less numerous, constituting 25.6 percent of the total assemblage of 226 pollen grains. However, the introduction of pollens from small grasses into the cave was favored because of their tendency to be collected by humans and animals as they traversed grassland or clearings before entering the cave. The arboreal species are dominated by oak (19 grains), pine (17 grains), juniper (16 grains), and ash. Two pollen grains of fir should be particularly noted; possibly they were carried by the wind from a distance. However, in one of the samples, stratigraphically the closest at 7.5 m (in excavation square D-8), six pollen grains of fir were found. These two samples are the only ones containing fir pollens, although the study analyzing the wood fragments indicates that the presence of fir relatively close to the cave seems possible.

The geographic situation of Shanidar cave at an altitude of about 765 m places the cave within the zone of marked vertical gradients; the nearest summits reach 1900 m. Numerous valleys cutting the mountains suggest the presence of microclimates related to the different slope exposures. The early Würm period, during which the older Mousterian deposits were laid down in a relatively humid environment, allowed for a certain diversity of flora. Dry grassland with more or less steppic plants such as Compositae liguliflores, *Ephedra*, Chenopodiaceae, and *Artemisia* were coexistent with high-altitude forests composed principally of conifers; at the same time ash and alder were sheltered in the river valleys and the drier oak and pine extended over the sunnier slopes.

As the botanical identification of the flowers in the grave of Shanidar IV is particularly important, it was necessary to attain the greatest possible precision as to their specific identity. The large number of pollen grains, more than 1500 for the composites, was a welcome aid.

This exhaustive study was conducted at Gröningen in collaboration with W. van Zeist, whose knowledge of Middle Eastern flora permitted a maximum number of identifications to be made. We recognize seven different plants in the form of flowers. An eighth raises a problem which is discussed below. The most numerous flowers are: *Achillea*-type, *Senecio*-type, *Centaurea solstitialis*-type, Liliaceae (*Muscari*-type), and *Ephedra altissima*-type.

Two other species could not be identified. The first species was very numerous but the very small, three-furrowed pollens had absolutely no ornamentation. This excluded attribution even to a botanical family.

In the above list, the first four species cited contain herbaceous plants, the flowers of which have very brilliant colors: blue for the *Muscari*, yellow for the *Senecio*, and more varied for the other Compositae. This does not apply to the *Ephedra*, whose flowers are very small and less visible. On the contrary, its flexible and ramose branches lend themselves rather well to the making of some sort of bedding on which the dead could have been laid.

Another problem has not been resolved, namely, the presence of many Malvaceae (type *Althaea*) pollen grains. Very large, covered with spikes, and extremely easy to spot in the slides, they occur in small numbers in the majority of the levels of the cave. But here, their quantity is excessive when viewed in relation to current plant distribution. One hundred thirty-four Malvaceae and 108 assorted pollen grains (not including the flowers) were found in sample 313, and 125 Malvaceae and 93 assorted pollen grains were found in sample 314. Although they never occur in clusters, the percentage of these isolated pollens is inexplicable for the moment.

Table 1 shows the clusters found in the three samples and the isolated pollen grains of the same species. The numbers indicated for the clusters are only minimum numbers as it is often impossible to do countings in these very compact masses. Those of the Compositae (types *Senecio*, *Achillea*, and *Centaurea*) usually form groups of from 2 to 15 grains but some contain approximately 30 grains. Certain unidentified pollens can be much more numerous.

Thus, during one of the early phases of the Würmian period, a more humid climate than during the present time favored a more dense arboreal vegetation in the vicinity of Shanidar cave. Nowadays, in the Zagros Mountains, the flowers which we have cited bloom in the months of May through June. It is possible that because of the climatic changes, a slight difference in the period of bloom exists; but one may assume that the placement of the Neanderthal man, Shanidar IV, at Shanidar cave on a bed of ramose branches and of flowers occurred more than 50,000 years ago between the end of May and the beginning of July.

ARLETTE LEROI-GOURHAN
Laboratoire de Palynologie,
Centre de Recherches Préhistoriques,
Musée de l'Homme, Paris, France

References and Notes

1. R. S. Solecki, *Science* **139**, 179 (1963).
2. A. Leroi-Gourhan, "Le Neanderthalien IV de Shanidar," *Bull. Soc. Prehist. Fr.* **65**, 79 (1968); R. S. Solecki incorporated the data from this paper in *Shanidar, The First Flower People* (Knopf, New York, 1971).
3. R. S. Solecki, personal communication.
4. J. L. Vernet made the analysis and botanical identifications.
5. M. Girard made this observation.

25 January 1975; revised 27 May 1975

Galilean Satellites and Jovian Energetic Particles

Abstract. *The observed infrared temperatures of the four Galilean satellites, Io, Europa, Ganymede, and Callisto, are inconsistent with their equilibrium temperatures. Since these satellites appear to have little or no atmosphere, the discrepancies may be explained as due to the heating of their surfaces by energetic particles from Jupiter's radiation belts. The required energy fluxes are not entirely unreasonable and decrease with the distance of the satellite orbit from Jupiter.*

It is postulated here that the observed infrared temperatures of the four Galilean satellites, Io, Europa, Ganymede, and Callisto, may only be understood if there is an additional source of energy other than the sun supplying heat to the surfaces of these satellites; one such additional source may be high-energy particles in Jupiter's magnetosphere. Furthermore, there is some indication that the effect diminishes with distance from Jupiter. The large sodium clouds observed about Io are undoubtedly connected with such bombardment.

Observations of the infrared temperatures of Io, Europa, Ganymede, and Callisto have been summarized by Morrison and Cruikshank (*1*) for the wavelength regions from 8 to 14 μm and 17 to 28 μm. The principal values listed in Table 1 are the means of the lowest and highest values for the tolerances of the measurements as quoted by Morrison and Cruikshank (*1*). The deviations of these mean values from the lowest and highest values are indicated by the parenthetical values in Table 1. All the temperatures listed represent equivalent blackbody temperatures for the satellite radii shown in Table 1, as taken from (*1*).

Table 2 lists satellite orbital radii (in Jupiter radii) as well as the visible phase integral (q_v), geometric albedo (p_v), and Bond albedo (A_v) as taken from Morrison and Cruikshank (*1*) [see (*2*) for definitions of these terms].

One may compute an equilibrium temperature for each satellite based on the values of A_v in Table 2. If a full spherical surface radiates back into space, the equilibrium temperature is given by

$$T_{eq} = \left[\frac{S_J(1-A_v)}{4\sigma\epsilon}\right]^{1/4} \quad (1)$$

where S_J is the solar constant at the orbit of Jupiter, σ is the Stefan-Boltzmann constant, and ϵ is the emissivity. Comparison of T_{eq} with the measured infrared temperatures must be made on the basis of $\epsilon = 1$, since the infrared temperatures are equivalent blackbody temperatures.

Equilibrium temperatures for $\epsilon = 1$ are listed in Table 3 as $T_{eq}(4)$. These temperatures are computed on the basis of a value for S_J of 5.12×10^4 erg cm^{-2} sec^{-1} and the A_v values in Table 2. Since the Galilean satellites may be locked to Jupiter, presenting one face toward the planet at all times, that side may receive little radiation from the sun, and one may argue that most of the reradiation back to space originates from part of the spherical surface. A lower limit may be a hemisphere. If only this much surface were radiating, the equilibrium temperature would be that given by Eq. 1 with a 2 replacing the 4 in the denominator. Equilibrium temperatures based on reradiation from only a hemisphere are listed in Table 3 as $T_{eq}(2)$; $T_{eq}(4)$ values in Table 3 refer to reradiation from the entire sphere.

All the equilibrium temperatures listed in Table 3 are less than the mean infrared temperatures in Table 1, regardless of whether reradiation is from a sphere or a hemisphere. One may attempt to explain this discrepancy as due to a greenhouse effect. However, the Galilean satellites appear to have little, if any, atmosphere. Thus, either the listed A_v values are too high so that the equilibrium temperatures are too low, or else solar radiation is insufficient to account for the observed temperatures. It is also conceivable that the radii used to compute the infrared temperatures are too small, but this appears unlikely as a major factor in view of the relatively small tolerances in the radii listed in Table 1. The disparity is not alleviated if one compares the equilibrium temperatures with the lower infrared temperatures (at 17 to 28 μm). The difference between the temperatures at 8 to 14 μm and the temperatures at 17 to 28 μm, when there is little atmosphere, is undoubtedly due to surface emissivity. Comparison is probably more appropriate with the higher infrared temperatures (at 8 to 14 μm) since these temperatures are closer to the true surface values which may indeed be still higher.

It may be that the A_v values in Table 2 are too high. Although one may have some confidence in p_v, the value of q_v is very uncertain and may have been overestimated. However, there is a limit to the correction, since A_v cannot be negative. (A negative A_v, or equivalently negative q_v or p_v, corresponds either to an internal energy source or to a source that is in addition to and separate from solar radiation.) When $A_v = 0$, $T_{eq}(4) = 122.6°$K and $T_{eq}(2) = 146°$K. It is not possible to account for measured infrared temperatures higher than these values with positive q_v values. The values of q_v required in order that $T_{eq}(2)$ match the temperature from 8 to 14 μm are listed as q' in Table 2. A negative value of q' is listed for Callisto. Only negative values of q' will bring about a match between $T_{eq}(4)$ and the measurement at 8 to 14 μm. Thus, it would be necessary that q_v vary from low values through zero to negative values, and it appears unlikely that A_v accounts for many of the discrepancies.

One possible explanation involves the influx of energy. On increasing the energy flux beyond that of solar radiation, one may find a value for S_J in Eq. 1, denoted as S, to equalize the temperatures. Using only the measurement from 8 to 14 μm (assuming that the temperature from 17 to 28 μm is due to surface conditions), one finds S (in units of S_J), the solar radiation flux, as given in Table 4 for both radiation from a hemisphere $[S(2)/S_J]$ and from a sphere $[S(4)/S_J]$.

It appears from the numbers listed in Table 4 that Io and Europa require about the same amount of additional energy, that Ganymede requires less, and Callisto still less. (The excess over unity represents the additional energy required.) Considering that the satellites are listed in order of distance from Jupiter in Table 2, it appears that the required energy decreases with distance from Jupiter. If this additional energy is due to particles in Jupiter's magnetosphere bombarding and heating the surfaces of these satellites, then these computations imply that the effect should diminish with distance from Jupiter. Pioneer 10 and Pioneer 11 measurements of high-energy particle fluxes (*3, 4*) show some decrease in flux with distance from Jupiter over the range of satellite orbital radii.

In the energy flux calculations in Table 4 it is assumed that there is a directed influx of energy similar to that from the sun. If the additional energy is due to particle bombardment, such bombardment may be from many directions. If all directions are involved, Eq. 1 becomes

$$T_{eq}(4) = \left(\frac{S_J + 4S_p}{4\sigma}\right)^{1/4} \quad (2)$$

where S_p is the energy flux absorbed by the surface due to particle bombardment. In the corresponding equation for $T_{eq}(2)$, the 4 in the denominator should be replaced by 2, although this substitution ignores some radiation from the neglected hemisphere. The actual condition relative to the directions of the particles probably lies somewhere between unidirectional and isotropic motion and varies with energy. Temperatures given by Eq. 2 are for isotropic particles. Table 4 also lists the values of $S_p(4)/S_J$ and $S_p(2)/S_J$, the latter for reradiation from a hemisphere and the former for a sphere.

The results presented here indicate that an energy source in addition to the sun's radiant energy may be heating the surfaces of the Galilean satellites. A likely source is the high-energy particles in the Jovian magnetosphere that undoubtedly bombard their surfaces. It also appears that this source decreases in intensity with distance from Jupiter, since there is a progressive decrease of needed energy flux with distance.

Table 1. Mean infrared temperatures and radii.

Satellite	Temperatures (°K)		Radius (km)
	8 to 14 μm	17 to 28 μm	
Io	138 (± 4)	126 (± 6)	1820 ± 10
Europa	129 (± 4)	121 (± 5)	1550 ± 150
Ganymede	144 (± 5)	137 (± 10)	2365 ± 25
Callisto	153 (± 5)	148 (± 12)	2500 ± 150

Table 2. Radiometric quantities.

Satellite	Orbital radius (Jupiter radii)	q_v	p_v	A_v	q'
Io	5.9	1	0.62	0.6	0.33
Europa	9.4	1	.68	.7	.53
Ganymede	15.0	0.8	.44	.4	.23
Callisto	26.3	.6	.19	.1	−1.83

Table 3. Equilibrium temperatures (in degrees Kelvin).

Satellite	$T_{eq}(4)$	$T_{eq}(2)$
Io	97.5	115.9
Europa	90.7	107.9
Ganymede	107.9	128.3
Callisto	119.4	142

Table 4. Required energy flux.

Satellite	$S(2)/S_J$	$S(4)/S_J$	$S_p(2)/S_J$	$S_p(4)/S_J$
Io	2	4	0.25	0.75
Europa	2.1	4.2	.275	.8
Ganymede	1.5	3.0	.125	.5
Callisto	1.38	2.76	.095	.44

The value of S_p for isotropic particle bombardment as given in Table 4 varies from about 5,000 erg cm^{-2} sec^{-1} for Callisto to about 14,000 erg cm^{-2} sec^{-1} for Io and Europa for equilibrium with the hemispheres of the satellites. For equilibrium over the entire sphere the energy flux required ranges from about 20,000 to about 40,000 erg cm^{-2} sec^{-1}, depending on the satellite. All of these fluxes are needed if the particles impinge on the satellites from all directions. Still greater fluxes are required for unidirectional particles.

The flux range 5,000 to 14,000 erg cm^{-2} sec^{-1} is about one order of magnitude greater than particle energy fluxes measured on the Pioneer 10 and Pioneer 11 missions (*4*). The larger required particle energy flux may be reasonable, however, since in the particle measurements the usually numerous kilovolt and lower-energy particles have not been included. On the other hand, particle energy fluxes required for equilibrium on a total spherical basis are of the order of two magnitudes greater than the measured flux rates. Such large fluxes may be questionable, unless by some peculiar coincidence Pioneer 10 and Pioneer 11 visited the vicinity of Jupiter during quiescent periods. Present information precludes any judgment on such a possibility. There may also be errors in the measurements that may mitigate the flux requirements. Some focusing of particles near the satellite may also be possible if there is some net charging of the satellites. These satellites may also be surrounded by plasma as for artificial earth satellites in the ionosphere.

In view of Io's apparently violent reactions to such particle bombardment with the release of sodium to the surrounding space, one should also look for similar clouds about the other Galilean satellites. Their much larger gravitational spheres of influence, however, may lessen the likelihood of such discoveries. Amalthea, closer to Jupiter and smaller than the Galilean satellites, may exhibit even more violent effects of bombardment than for the Galilean satellites.

STANLEY H. GROSS
Department of Electrical Engineering and Electrophysics, Polytechnic Institute of New York, Farmingdale 11735

References and Notes

1. D. Morrison and D. P. Cruikshank, *Space Sci. Rev.* **15**, 641 (1974).
2. Albedo is a synonym for reflectivity, but it is usually modified by qualifying words. The Bond albedo is the ratio of the total light power reflected in all directions from a body to the total light power incident on it in a collimated beam. It is the fraction of the incident solar flux that is not absorbed. The Bond albedo is the product of the geometric albedo and the phase integral. The geometric albedo is the ratio of the power per unit solid angle per unit projected area at full phase (phase angle is zero) to the power per unit solid angle per unit projected area of a perfectly diffusing disk in the same position and with the same apparent size as the planet or satellite. The disk is taken to be normal to the source of illumination (the sun). The perfectly diffusing disk absorbs no power and scatters all incident flux according to Lambert's law. The phase angle is the planet- or satellite-centered angle between the source of illumination (the sun) and the observer (or detector). The phase integral is the ratio of power scattered in all directions to that scattered at zero phase per unit solid angle. For a nonspecialist, additional information on this terminology may be found in: S. K. Runcorn *et al.*, Eds., *International Dictionary of Geophysics* (Pergamon, Oxford, 1967), vol. 1; R. W. Fairbridge, Ed., *Encyclopedia of Atmospheric Sciences and Astrogeology* (Reinhold, New York, 1967).
3. J. A. Simpson, D. C. Hamilton, G. A. Lentz, R. B. McKibben, M. Perkins, K. R. Pyle, A. J. Tuzzolino, J. J. O'Gallagher, *Science* **188**, 455 (19 → J. H. Trainor, F. B. McDonald, D. E. Stilwell, B. J. Teegarden, W. R. Webber, *ibid.*, p. 462; J. A. Van Allen, B. A. Randall, D. N. Baker, C. K. Goertz, D. D. Sentman, M. F. Thomsen, H. R. Flindt, *ibid.*, p. 459.
→ R. W. Fillius, C. E. McIlwain, A. Mogro-Campero, *ibid.*, p. 465.
5. This work was supported in part by NASA grant NGR-33-006-068.

27 May 1975; revised 2 July 1975

Magnetotelluric Sounding of Permafrost

Abstract. *The audio-frequency magnetotelluric method was used to sound a permafrost region in the Mackenzie delta in the Northwest Territories. A simple two-layer model consisting of a high electrical resistivity layer overlying less resistive material gave interpreted depths in agreement with those determined by drilling. The summer active layer was transparent even at high sounding frequencies.*

The mapping of permafrost thickness in the Arctic is an important problem having applications ranging from the construction of pipelines to the interpretation of seismic data. Electrically, the transition from frozen to unfrozen earth is generally accompanied by a significant decrease in resistivity (*1*). The problem of measuring permafrost thickness then becomes one of measuring the depth to this electrical interface.

Audio-frequency magnetotellurics (AMT), an extension of the basic magnetotelluric method first proposed by Cagniard (*2*), is a system which utilizes naturally occurring telluric currents that are induced by distant lightning discharges. These "sferics" propagate in the earth-ionosphere cavity and with sensitive instrumentation can be detected many thousands of miles away. By use of grounded electric dipoles 100 feet (~ 30 m) in length and a broadband induction coil, coherent sferic pulses in the electric and magnetic fields are passed through narrow band pass filters and the ratio of the average electric field strength to the average magnetic field strength is electronically determined (*3*).

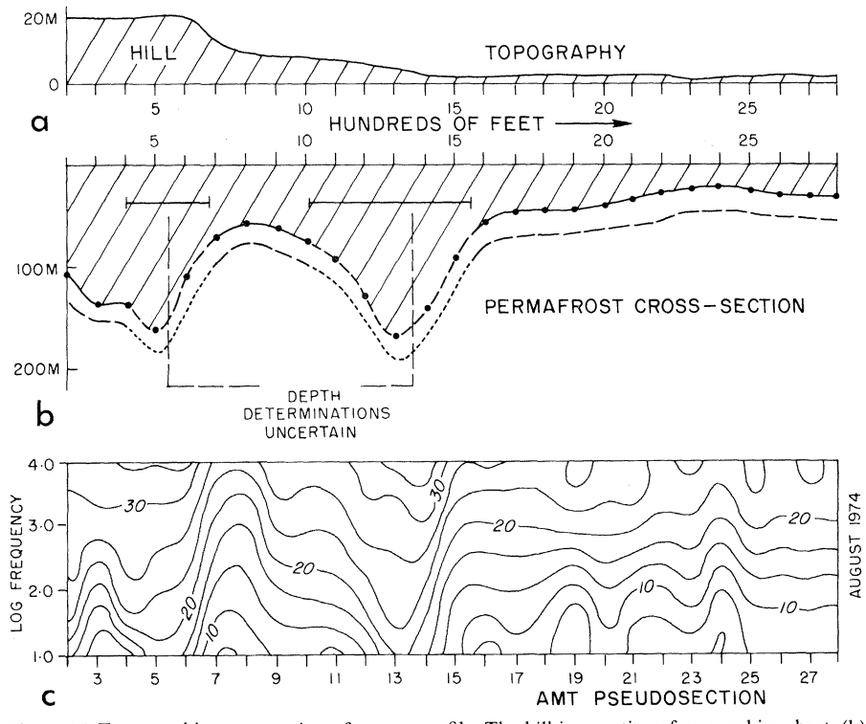

Fig. 1. (a) Topographic cross section of survey profile. The hill is a vestige of an areal ice sheet. (b) Permafrost cross section determined at 10 khz using a two-layer model. (c) Pseudosection representation of data indicating both lateral and vertical variations in resistivity. Labeled contours are intervals of 10 log ρ_a. The electric field was measured across the profile.